Location matters: Offset in tissue-engineered vascular graft implantation location affects wall shear stress in porcine models

Jacqueline Contento, BSE,[a] Paige Mass, BS,[a] Vincent Cleveland, MS,[a] Seda Aslan, MS,[b] Hiroshi Matsushita, MD,[c] Hidenori Hayashi, MD,[c] Vivian Nguyen, PhD,[d] Keigo Kawaji, PhD,[d] Yue-Hin Loke, MD,[a] Kevin Nelson, PhD,[e] Jed Johnson, PhD,[e] Axel Krieger, PhD,[b] Laura Olivieri, MD,[a] and Narutoshi Hibino, MD, PhD[c,f]

ABSTRACT

Objective: Although surgical simulation using computational fluid dynamics has advanced, little is known about the accuracy of cardiac surgical procedures after patient-specific design. We evaluated the effects of discrepancies in location for patient-specific simulation and actual implantation on hemodynamic performance of patient-specific tissue-engineered vascular grafts (TEVGs) in porcine models.

Methods: Magnetic resonance angiography and 4-dimensional (4D) flow data were acquired in porcine models (n = 11) to create individualized TEVGs. Graft shapes were optimized and manufactured by electrospinning bioresorbable material onto a metal mandrel. TEVGs were implanted 1 or 3 months postimaging, and postoperative magnetic resonance angiography and 4D flow data were obtained and segmented. Displacement between intended and observed TEVG position was determined through center of mass analysis. Hemodynamic data were obtained from 4D flow analysis. Displacement and hemodynamic data were compared using linear regression.

Results: Patient-specific TEVGs were displaced between 1 and 8 mm during implantation compared with their surgically simulated, intended locations. Greater offset between intended and observed position correlated with greater wall shear stress (WSS) in postoperative vasculature ($P < .01$). Grafts that were implanted closer to their intended locations showed decreased WSS.

Conclusions: Patient-specific TEVGs are designed for precise locations to help optimize hemodynamic performance. However, if TEVGs were implanted far from their intended location, worse WSS was observed. This underscores the importance of not only patient-specific design but also precision-guided implantation to optimize hemodynamics in cardiac surgery and increase reproducibility of surgical simulation. (JTCVS Open 2022;12:355-63)

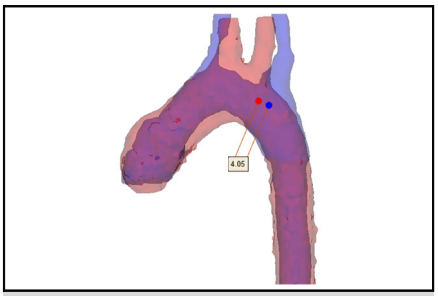

Pre- (*red*) and postoperative (*blue*) vasculature overlayed to calculate graft offset.

CENTRAL MESSAGE

Tissue-engineered vascular grafts have the potential to improve hemodynamics when implanted in their intended locations, emphasizing the importance of precision-guided implantation during surgery.

PERSPECTIVE

As the use of patient-specific tissue-engineered vascular grafts increases in patients with congenital heart disease, we must acknowledge how precise surgical implantation helps to further optimize their hemodynamic benefits by reducing wall shear stresses along vascular endothelial tissue.

From the [a]Department of Cardiology, Children's National Hospital, Washington, DC; [b]Laboratory for Computational Sensing and Robotics, Johns Hopkins University, Baltimore, Md; [c]Division of Cardiac Surgery, Department of Surgery, University of Chicago, Chicago, Ill; [d]Department of Biomedical Engineering, Illinois Institute of Technology, Chicago, Ill; [e]Nanofiber Solutions, LLC, Dublin, Ohio; and [f]Department of Cardiovascular Surgery, Advocate Children's Hospital, Oak Lawn, Ill.

This project is supported by National Institutes of Health award numbers K25HL141634, R01HL143468, R21HD090671, and R33HD090671. The content is solely the responsibility of the authors and does not represent the official views of the National Institutes of Health.

Read at the 102nd Annual Meeting of The American Association for Thoracic Surgery, Boston, Massachusetts, May 14-17, 2022.

Received for publication May 19, 2022; revisions received July 28, 2022; accepted for publication Aug 8, 2022; available ahead of print Sept 14, 2022.

Address for reprints: Narutoshi Hibino, MD, PhD, Section of Cardiac Surgery, Department of Surgery, The University of Chicago, Advocate Children's Hospital, 5841 S Maryland Ave, Room E500B, MC5040, Chicago, IL 60637 (E-mail: nhibino@bsd.uchicago.edu).

2666-2736

https://doi.org/10.1016/j.xjon.2022.08.006

Abbreviations and Acronyms

AR = augmented reality
CFD = computational fluid dynamics
CHD = congenital heart disease
4D = four-dimensional
LPA = left pulmonary artery
MPA = main pulmonary artery
MRA = magnetic resonance angiography
MRI = magnetic resonance imaging
PA = pulmonary artery
RPA = right pulmonary artery
SCA = subclavian artery
αSMA = α-smooth muscle actin
STL = stereolithography
TEVG = tissue-engineered vascular graft
WSS = wall shear stress

Congenital heart disease (CHD) affects 1% of live births worldwide and is the leading cause of death in newborns.[1] For children with severe CHD, surgeons implant commercially available grafts to correct narrowed blood vessels or bypass defective heart chambers. The current standard of care is using off-the-shelf grafts, but these can produce suboptimal hemodynamics and are subject to early failure.[2] Additionally, grafts cannot grow with the patient and always require replacement. Patients with repaired CHD often face complications, such as exercise intolerance, ventricular dysfunction, arrhythmias, cyanosis, or major embolic events.[3] Thus, there is a clinical need for patient-specific grafts designed to improve congenital vascular repair.

We developed patient-specific tissue-engineered vascular grafts (TEVGs) using magnetic resonance imaging (MRI) and subsequent 3D design to improve hemodynamics within unique patient anatomies. These customized biodegradable scaffolds promote cellular proliferation and maturation with potential for growth and anatomic reconstruction.[4,5] Preclinical studies of patient-specific TEVGs in sheep models have shown favorable outcomes, such as decreased thrombogenicity,[6] and TEVGs were also used to treat congenital pulmonary artery (PA) stenosis in 2 children, and exhibited safe histological and mechanical properties.[7]

A patient-specific design approach requires image segmentation, computer-aided design modifications guided by computational fluid dynamics (CFD) simulations and electrospinning to create a customized conduit.[8] CFD simulation explores various surgical solutions while predicting postoperative hemodynamics like wall shear stress (WSS) and energy loss.[9] CFD results reveal that optimized grafts outperform standard grafts and improve hemodynamic parameters, demonstrating the potential to improve CHD surgery.[10]

Higher levels of WSS (>10 Pa) have been shown to induce specific changes in endothelial cell behavior and exacerbate inflammation.[11] Lower levels of WSS (<1 Pa) are typically associated with worse pulmonary vascular remodeling and pulmonary arterial hypertension.[12,13] WSS has been implicated in repaired aortic coarctation patients, with high WSS correlated with reduced growth in the transverse arch.[14] Research also suggests that abnormal WSS promotes the development and rupture of high-risk plaques, which might lead to atherosclerosis and myocardial infarction.[15,16] From a histological standpoint, regions of low and high WSS correspond to medial thickening and degradation, respectively.[17] Because of these clinical implications and profound effects on tissue biology, WSS is at the forefront of cardiovascular research and a key target in CFD optimization. Energy loss is also a consideration because of its correlation to abnormal arterial flow, evident in viscous energy losses in dilated aortas (>2 mW) and aortic stenosis (>10 mW).[18]

Although CFD simulation is advanced in predicting surgical outcomes, little is known about the accuracy of surgical placement of patient-specific designed grafts. Our aim was to determine whether the location of TEVG implantation matters, and if so, the implications. Therefore, the primary objective of this study was to evaluate the offset in TEVG implantation location compared with its CFD surgical simulated position. The secondary objective was to determine if the location of the implanted TEVG affects hemodynamic performance of the postoperative blood vessel in porcine models. We hypothesized that precise implantation of TEVGs in their intended positions would result in improved hemodynamic performance than TEVGs with greater offsets.

METHODS

3D Model Design

All procedures were performed at the University of Chicago Medical Center and approved by the Institutional Animal Care and Use Committee (72605; approved October 24, 2019). All animals received humane care in compliance with the Guide for the Care and Use of Laboratory Animals (Facility RRID:SCR_021806). Fourteen-week-old pigs weighing 20 to 30 kg underwent cardiac magnetic resonance angiography (MRA) with a 32-channel torso array on a 3.0 T magnet (Philips Ingenia) at approximately 1 month before implantation surgery (Figure 1, *A*). For the MRA acquisition we used a four-dimensional (4D)-TRAK sampling scheme over the cardiothoracic region using a sagittal view, with the following acquisition parameters: repetition time/time to echo/fractional anisotropy = 3.8/1.6 ms/25°, field of view = 410 × 410 × 240 to 250 mm^3, spatial resolution = 0.9 × 0.9 × 6 mm^3, and a compressed SENSE acceleration with reduction factor = 4. For the two 4D flow sequences, the velocity encoding gradients of 250 and 350 cm/s were matched to the following acquisition parameters: repetition time/time to echo/fractional anisotropy = 3.9/2.1 ms/14°, field of view = 284 × 284 × 120-160 mm^3, spatial resolution = 0.85 × 0.85 × 1.7 mm^3, reconstructed cardiac phases = 20 per heartbeat with automatic k-space view-sharing, and a compressed SENSE acceleration with reduction factor = 3.5 to 4.

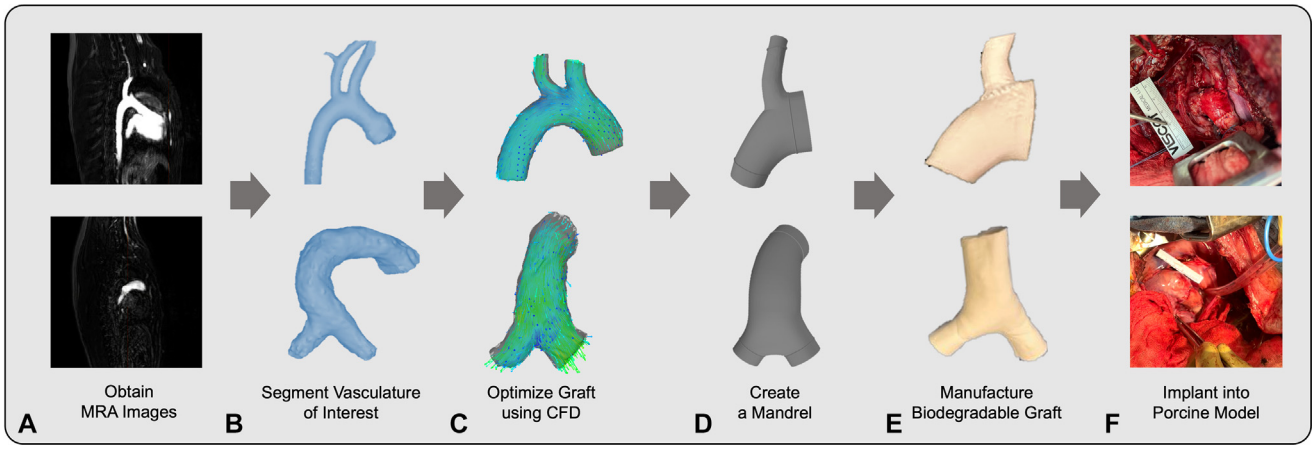

FIGURE 1. Workflow of tissue engineering graft manufacturing for aortic (*top*) and pulmonary artery (*bottom*) grafts. A, Obtaining magnetic resonance angiography (*MRA*) images 1 month before implantation. B, Constructing 3D digital models using segmentation software. C, Optimizing graft design using computational fluid dynamics (*CFD*) techniques. D, 3D printing metal mandrels for scaffold fabrication. E, Electrospinning the biodegradable polymer graft. F, Implanting the graft into a porcine model.

MRA images were segmented using Mimics (Materialise) to identify the vasculature (either aorta or PA bifurcation). To reduce subjectivity, automatic thresholding via the Otsu method using Matlab (MathWorks) was used to identify the blood pool in each MRA slice.[19] The final segmentation was converted into a 3D digital model and smoothed. To account for growth during the 1-month period between imaging and implantation, the vessel model was expanded by 5% uniformly using the scaling tool in 3-matic (Materialise). This percentage was determined on the basis of the growth curve of the mixed Yorkshire and Landrace porcine model and observed vessel diameter growth over a 1-month period in previous work.[5] The resulting model was exported as a stereolithography (STL) file (Figure 1, *B*).

A graft was created on the basis of the exported vessel and optimized to enhance hemodynamic performance (Figure 1, *C*) by exploring graft geometries, performing high-fidelity CFD simulations, and using machine learning methods on the basis of preoperative 4D flow data and methods, consistent with our previous work in this area.[9,20,21] Our iterative CFD processes continued until acceptable thresholds of WSS and energy loss were obtained (1-10 Pa[11] and <2 mW[18] in arterial flow, respectively). The optimized model was exported as an STL file for electrospinning.

Scaffold Fabrication

The STL file was modified for the electrospinning setup and removal of the electrospun polymer graft.[22] Then, the modified graft was 3D-printed in stainless steel with direct metal laser sintering at an external printing house (Protolabs or Xometry; Figure 1, *D*). The steel mandrel was coated in a biodegradable nanofiber material composed of a 1:1 ratio of polycaprolactone and poly-L-lactide-co-ε-caprolactone (Nanofiber Solutions). These polymer fibers were deposited on the mandrel during electrospinning while maintaining high voltage. When completed, the mandrel was disassembled, and the electrospun biodegradable graft was removed and placed in a standard Tyvek pouch (Figure 1, *E*). The graft was sterilized in low temperature with vaporized hydrogen peroxide and ozone (STERIZONE VP4; Getinge).[23]

In Vivo Graft Implantation

Eleven porcine models were subject to graft implantation cardiovascular surgery 1 month after preoperative imaging. Postoperative imaging was either acquired within 2 days after surgery for acute studies (n = 8) or 2 months for chronic studies (n = 3). Five of the animals received an aortic graft and 6 received PA bifurcated grafts. Each biodegradable graft included extensions, marked by ridges, to indicate where the graft should be sutured. The aortic grafts contained 3 ridges, located at the ascending aorta, descending aorta, and subclavian artery (SCA). The PA grafts also contained 3 ridges: 1 at the main PA (MPA), left PA (LPA), and right PA (RPA). Each graft was uniquely shaped and sized to their respective implantation sites using the TEVG manufacturing work flow detailed in Figure 1.

Graft implantation surgery was performed through a left thoracotomy with general anesthesia after removal of 1 rib to increase exposure (Figure 1, *F*). Aortic grafts were implanted in the descending aorta only (n = 2), or in the descending aorta and left SCA (n = 3). The inclusion of the SCA was predetermined in the design process. Aortic grafts including the SCA were anastomosed distal of the brachiocephalic trunk, whereas grafts without a branch were placed distal of the left SCA. This procedure was performed with partial bypass using 2 cannulas connected to the ascending aorta and distal of the descending aorta to provide the lower body perfusion while clamps were in place. The PA grafts were implanted from the MPA to the branch PA after removal of the central PA portion. This procedure was performed using cardiopulmonary bypass. All pigs woke up after the surgery and were extubated in the operating room. Grafts were explanted at acute (within 2 days; n = 8) or chronic (2 months; n = 3) phases after the surgery.

Center of Gravity Analysis

Postoperative MRA and 4D flow data were reacquired immediately before explantation using matched acquisition as the preoperative imaging, and the obtained volumetric data sets were segmented with identical methods as described previously. The preoperative and postoperative vasculature segmentations were aligned in space using the automatic global registration feature in 3-matic. To account for growth between pre- and postoperative imaging time points (1 month or 3 months), preoperative images were scaled to postoperative size according to species-specific estimated growth curves.[24] Two copies of the designed graft on the basis of preoperative imaging were added to the workspace. One of the grafts was aligned using global registration to the preoperative image, what we referred to as the "ideal" graft position. Conversely, the other graft was aligned to the postoperative image, what we referred to as the "observed" graft position.

To quantify this offset in 3D space, an automated center of gravity analysis was performed using the proprietary 3-matic on the basis of previous methodologies.[25,26] This software uses mesh fit programming to

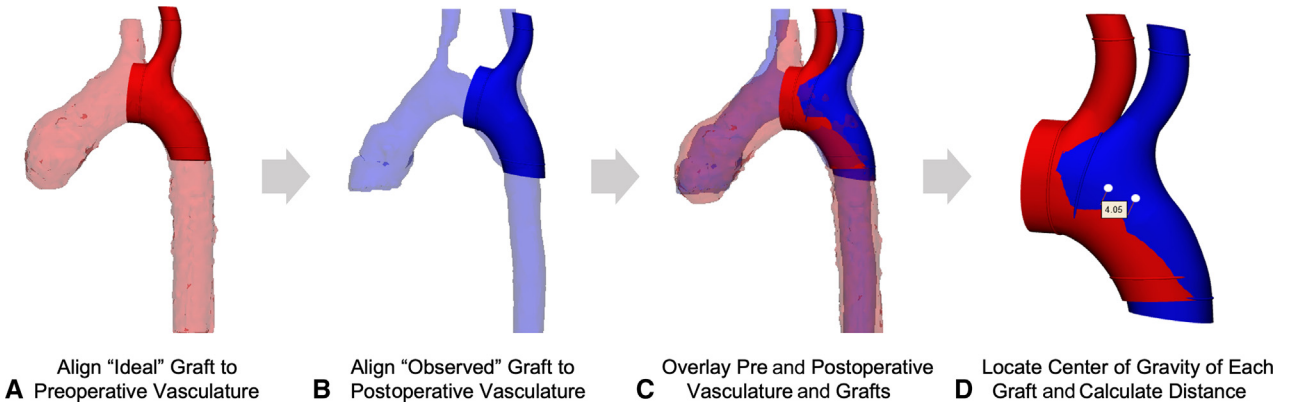

FIGURE 2. Work flow for center of gravity analysis for an aortic graft. A, Aligning preoperative vasculature and graft. B, Aligning postoperative vasculature and graft. C, Overlaying pre- and postoperative vasculature and grafts. D, Determining offset by calculating distance between centers of gravity. *Red* represents the preoperative model, whereas *blue* represents the postoperative model.

determine the center of gravity of each model selected. Grafts were selected, instead of the vasculature, because they have the same mass and shape to allow for comparison. Finally, the measure distance tool in 3-matic was used to identify the offset between the 2 center of gravity points in 3D space (Figure 2).

Implanted Graft Hemodynamic Analysis

Postoperative 4D flow images of the implanted graft were exported for further analysis, similar to our previously published methods.[27] The hemodynamic factors of WSS, energy loss, right-handed helicity, and vorticity were measured using iTFlow (Cardio Flow Design) as defined by standard landmarks segmented in previous work.[28] In the aorta samples, measurements and average hemodynamics were calculated across the whole vessel, which includes the ascending aorta, the transverse arch, and the descending aorta. The ascending aorta was defined as the region from the top of the aortic root to the first head vessel. The transverse arch was the region from the first head vessel to the second head vessel. The descending aorta was defined as the region from the second head vessel continuing down to 1 cm below the starting plane of the ascending aorta. The aorta flow rates were measured at the beginning of the ascending aorta and at the end of the descending aorta.

The measurements and average hemodynamics of the PA samples were also calculated across the whole vessel, including the MPA, LPA, and RPA segments. The MPA was defined as the region from the end of the PA curve up to the junction of the LPA and RPA. The RPA was the region from the PA junction to the first branch on the RPA. The LPA was defined as the region of the LPA from the junction with the RPA equidistance as the RPA. The PA flow rates were measured at the beginning of the MPA, the beginning of the RPA, and the beginning of the LPA. All measurements were visualized in iTFlow for the identification of regions of interest (Figure 3). Although it was not possible to differentiate the TEVG from the native vessels using iTFlow, the defined regions were sized to include the entire graft.

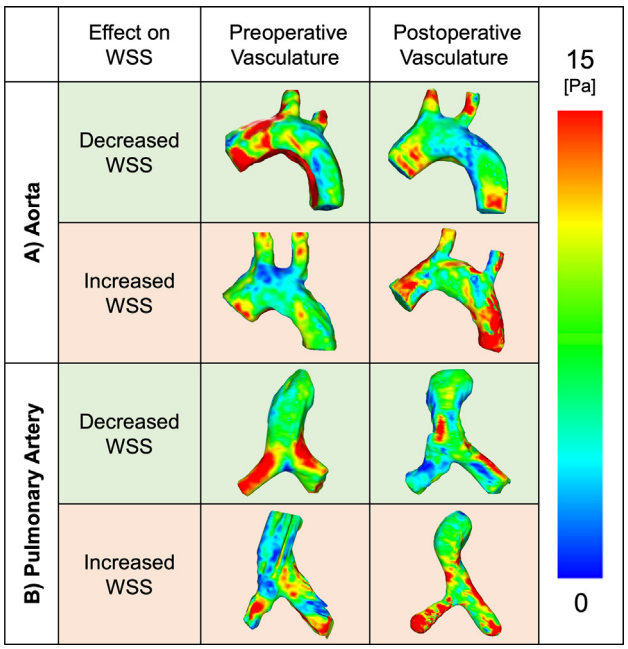

FIGURE 3. Wall shear stress (*WSS*) measured in pascals of tissue-engineered vascular graft in porcine models. Pre- and postoperative WSS in (A) aorta and (B) pulmonary artery bifurcated models. *Top rows* (*green*) represent an improvement in WSS, whereas *bottom rows* (*red*) represent a worsening in WSS.

Histological Analysis

Chronic phase grafts were explanted, fixed in 10% formalin for 24 hours, and then embedded in paraffin. Standard histology was completed using hematoxylin and eosin stains. Immunohistochemistry was performed using α-smooth muscle actin (αSMA; 1:1600 M0851 Dako). Detection of antibody binding was performed using biotinylated secondary antibodies (Vector Laboratories), followed by incubation with streptavidinated horseradish peroxidase (Vector Laboratories). A chromogenic reaction with 3,3-diaminobenzidine (Vector Laboratories) was performed for the development of immunohistochemistry. Counterstaining of the nuclei was performed with Gill's hematoxylin (Vector Laboratories).

Statistical Analysis

Simple linear regression was performed to assess the associations between TEVG implantation offset and hemodynamic parameters. WSS, energy loss, helicity, and vorticity are presented as percent differences calculated using the following equation. R^2 and P values were calculated using Prism Version 8 (GraphPad Software).

$$\%Difference = \frac{Postoperative - Preoperative}{(Postoperative + Preoperative)/2}$$

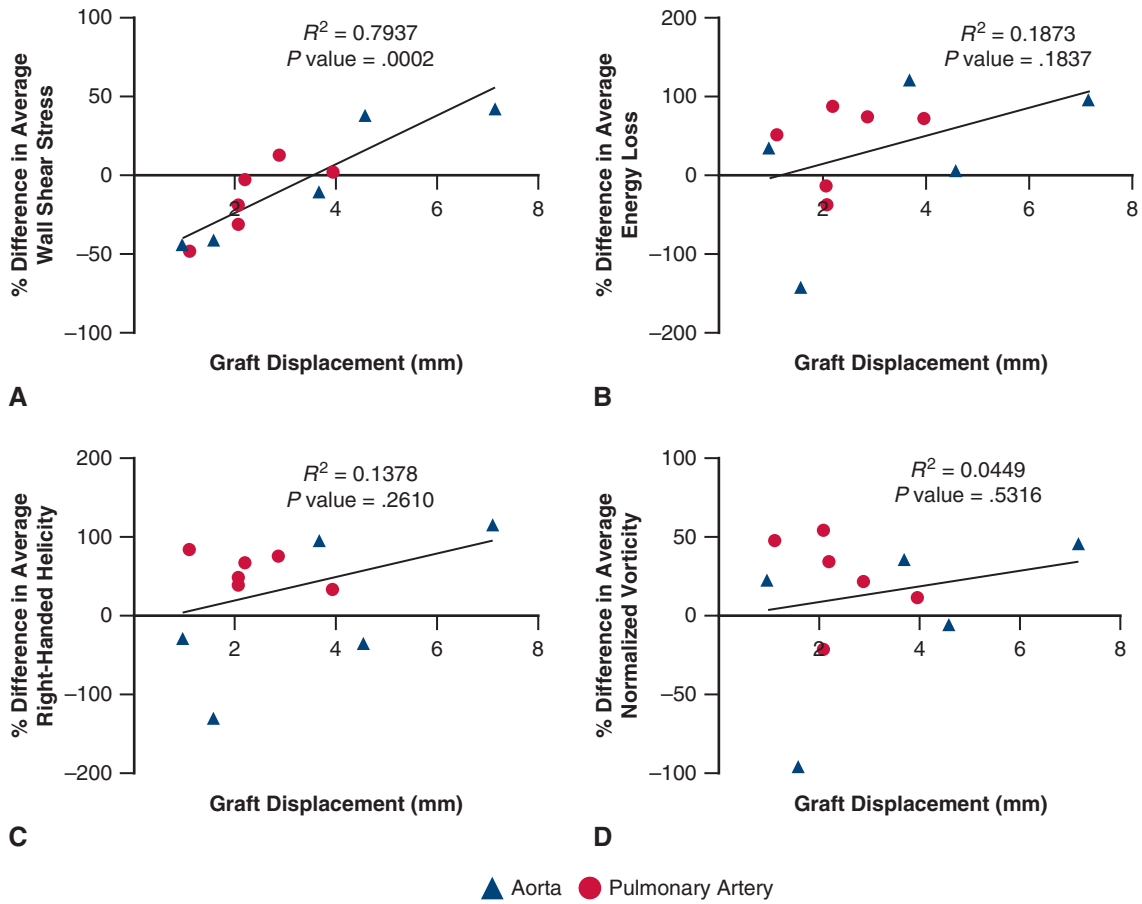

FIGURE 4. Graft displacement (mm) versus percent difference in average wall shear stress (A) energy loss, (B) helicity, and (C) and (D) vorticity within the aorta and pulmonary artery grafts.

RESULTS

Anatomical Observations

Eleven (n = 11) pigs underwent graft implantation surgery and postoperative analysis. After MRI, the animals were euthanized, and grafts were explanted between 1 week and 2 months after the surgery. Growth periods are shown in Figure E1 (aorta: n = 5 at 1 month; PA: n = 3 at 1 month and n = 3 at 3 months). There were no stenosis or dilated grafts.

Our center of gravity results showed that patient-specific TEVGs were displaced by approximately 1 to 8 mm during implantation surgery compared with their intended locations used in CFD surgical simulations. On average, the aortic grafts exhibited greater displacement and wider variety within measurements (3.82 ± 2.77 mm) compared with the PA bifurcated grafts (2.30 ± 1.19 mm).

Effects of Displacement on Hemodynamics

Next, we analyzed the effects of the calculated offset on hemodynamic performance, including WSS, energy loss, helicity, and vorticity (Figure 4). Data for the 11 porcine models showed a positive correlation between displacement and average WSS (R^2 = 0.79). This trend was observed within the aortic and PA grafts. Thus, we concluded that greater offset between the intended and observed position led to a higher average WSS over postoperative vasculature ($P < .01$). Furthermore, less offset between intended and observed positions not only led to decreased average WSS but improvements in WSS between preoperative and postoperative vasculature (as indicated by negative values in Figure 4, *A*).

Conversely, there were no strong correlations between displacement and energy loss, helicity, and vorticity ($P = .18$, $P = .26$, and $P = .53$, respectively). Therefore, grafts that were implanted closer to their intended locations showed positive results on hemodynamic performance in terms of WSS, but not the other parameters. Displacement, WSS, energy loss, helicity, and vorticity data for all 11 porcine models are shown in Figure E1.

Effects of WSS on Histology

Histological analysis was performed on chronic cases only (n = 3). Porcine subject 4 was excluded from this

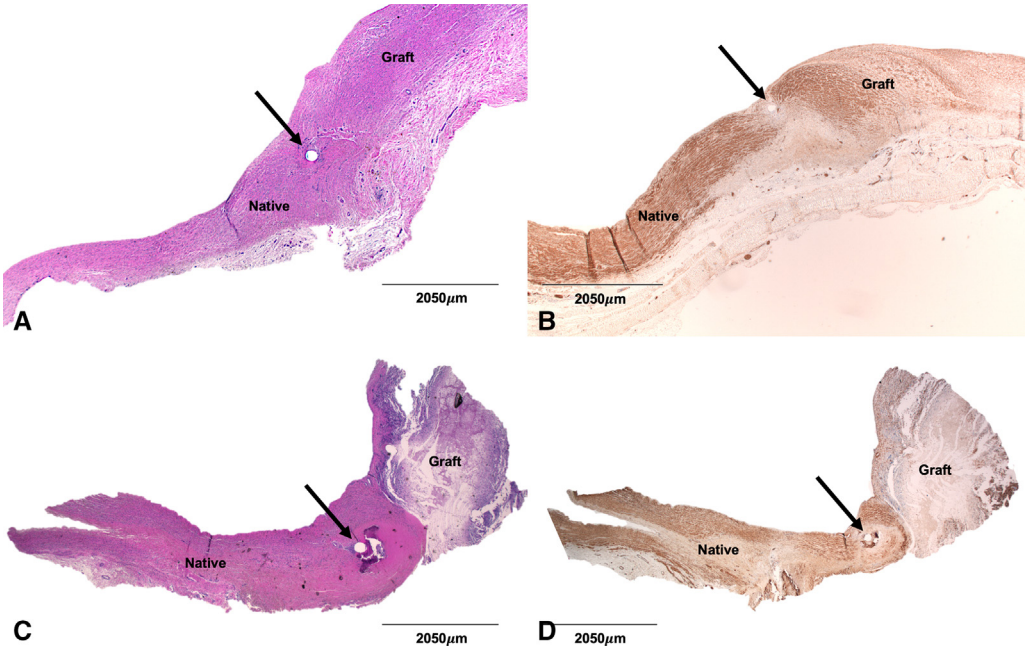

FIGURE 5. Histology of pulmonary artery graft 5 shown through an (A) hematoxylin and eosin stain and (B) α-smooth muscle actin markers. Histology of pulmonary artery graft 6 shown through a (C) hematoxylin and eosin stain and (D) α-smooth muscle actin markers. The *arrow* indicates the needle hole to suture the graft. *The region left of the needle hole* represents native tissue, and *the region right of the needle hole* represents the tissue-engineered vascular graft.

data set because of damage that led to poor data quality. Histological analysis of the PA of porcine subject 5 showed neotissue formation of smooth muscle layers similar to native tissue. 4D flow MRI data showed a reduction in WSS between presurgical and 2-month postsurgical imaging (Figure 5, *A* and *B*).

For comparison, histological analysis was also performed on the PA of porcine subject 6, which showed higher WSS at 2 months postoperative than preoperative. In Figure 5, *C* and *D*, we see intimal hyperplasia due to vascular wall inflammation. Medial thinning occurred as a result, evident in the slight narrowing of the postoperative blood vessel shown in Figure E1, displacement figure of porcine subject 6.

DISCUSSION

Center of gravity analysis is a novel method for determining location. The 3-matic center of gravity analysis used in this study has been validated in other works[25,26] but has yet to inform surgical procedures in the 3D space. This process allowed us to determine the intended location for the TEVG used in surgical simulation and CFD analysis, as well as the observed location of the implanted TEVG within the porcine model. Consequently, we calculated the difference between the intended and observed locations to determine the offset that occurs during cardiovascular surgery. We saw greater displacement in aortic grafts, which might be due to the more constrained operating space of PAs compared with aortas.

The results of this study validate the benefit of patient-specific TEVGs when implanted in vivo in porcine models. When the TEVG was implanted closer to the intended position that was used in surgical simulation and CFD analysis, results show improved WSS (decreased WSS in the postoperative case vs the preoperative). In other words, patient-specific TEVGs aim to reduce WSS when implanted correctly, revealing the importance of patient-specific design in optimizing hemodynamics. We found no correlations relating TEVG implantation location and the other hemodynamic parameters of energy loss, vorticity, and helicity.

However, it was also shown that greater TEVG displacement of the implanted TEVGs had negative effects on hemodynamics, increasing WSS in the postoperative cases. As shown in the histological analysis, high WSS produced intimal hyperplasia in a PA TEVG graft compared with its native tissue. Conversely, a PA sample with lower WSS showed similar formation of smooth muscle layer to its native tissue. In future work we will investigate additional histological analyses in other tissue samples, because our limited findings might not be representative for the whole cohort. Overall, the location of the TEVG matters, and precision-guided implantation must be improved for patient-specific design to be its most effective.

Considering that high WSS ranges are linked to thrombosis formation,[11] our engineers focused on minimizing WSS in areas with the highest values when designing the

graft shape. Although helicity and vorticity have been studied extensively as markers of secondary flow formations and efficiency, there is no relationship established between a specific range of these values to any clinical parameter. The animals included in our study were healthy pigs with normal aorta and PA anatomies, whereas vortex and helix formations are commonly seen in abnormal valve, stenosis, and aneurysmal dilatation.[29,30] Last, geometrical differences between the designed and native anatomies were not significant enough to create major changes in vorticity and helicity; thus, we did not consider optimizing these parameters when designing the TEVGs.

CFD surgical simulations show promising insights into improving cardiovascular surgery as a surgical planning tool. By simulating different models, CFD can reveal a TEVG configuration that can bypass surgical issues and optimize hemodynamic performance. However, the greatest challenge is for surgeons to reproduce the suggested operation with similar outcomes. For example, Trusty and colleagues[31] showed that CFD-optimized Fontan conduits might still have deviations in predicted hepatic flow distribution, as a result of offset error during implantation. Such fidelity is only achieved by the surgeon's involvement in preoperative modeling to create a surgically feasible configuration and commitment to precisely execute in the operating room. Methodological improvements are necessary to increase the overall accuracy and reproducibility of surgical planning; otherwise, the benefits of CFD will not be observed.

This study is limited because of its small sample size of 11 porcine models. The porcine animal model has an expedited growth curve compared with humans, thus requiring the design to account for estimated growth between the preoperative imaging and date of implantation. This growth was estimated to be 5% on the basis of the animal growth curve and previously observed vessel growth in a 1-month study in the same breed[5]; however, this is an estimation and does not account for varied growth differences between cross-sectional and linear growth of the vessel.[32] It is possible that differences in vessel diameter due to misapproximation of the growth added confounding factors to the hemodynamic analysis. Future work should be considered to estimate growth of the vessel more accurately.

Porcine models endured varying healing times between surgery and postoperative imaging. Cases with longer periods of time, as opposed to more limited healing times of <2 days, experienced more vasculature growth, which might have introduced confounding variables. For instance, larger porcine models inherently possess higher WSS because of higher cardiac output and greater sustained flow.[33] This might also explain why 8 of the 11 porcine subjects had positive percentage differences in energy loss, helicity, and vorticity. Another reason might be that all porcine subjects were considered healthy, without any defects that would have reduced hemodynamic parameters, so optimization was minimal on theoretically ideal vessels. Last, other excluded models included those with surgical issues, such as stenosis, which resulted in extremely high WSS regardless of TEVG placement. Thus, the estimation of graft implantation location might not have perfectly assessed growth or accounted for surgical issues.

Unfortunately, there is a unique potential error of surgical implantation in cardiac procedures due to decompressed structures during cardiopulmonary bypass surgery. Because of this issue and its complications on hemodynamic performance, a tool is needed to ensure precision during implantation cardiac procedures. Optimal repair for complex CHD requires high demand on 3D anatomical imagination, so the use of augmented reality (AR) might serve as a potential solution. Preliminary studies have shown that using holograms as a surgical planning tool for CHD might have a high diagnostic value and contribute to understanding complex morphology.[34] Other AR surgical simulators have incorporated haptic feedback for a more immersive learning experience for surgeons.[35] Future work should investigate the applications of AR technology to aid precise graft implantation efforts during cardiac procedures.

CONCLUSIONS

Patient-specific TEVGs are designed for precise locations to help optimize hemodynamics. The greater the difference between the intended versus actual implantation location of a TEVG, the worse the observed hemodynamic performance in terms of WSS. This underscores the importance of not only patient-specific design but also precision-guided implantation to optimize hemodynamics in cardiac surgery. There still presents a need for a precision tool to mimic implantation locations used in surgical simulations.

Conflict of Interest Statement

J. Johnson, A. Krieger, and N. Hibino are inventors listed on International Patent WO/2017/035500Al (Patient-Specific Tissue Engineered Vascular Graft Utilizing Electrospinning). The patent filing has been disclosed for grant applications and to institutions. J. Johnson and N. Hibino are equity holders in Nanofiber Solutions. All other authors reported no conflicts of interest.

The *Journal* policy requires editors and reviewers to disclose conflicts of interest and to decline handling or reviewing manuscripts for which they may have a conflict of interest. The editors and reviewers of this article have no conflicts of interest.

The authors thank the University of Chicago Animal Resources Center (RRID:SCR_021806), especially the Carlson Large Animal Clinic Staff, Dr Allison Ostdiek, Dr Darya Mailhiot, Jenny McGrath, Alyssa Brown, Erika Becerra, and Pierre Latalldi for their assistance with animal surgery and housing. They also thank

the University of Chicago Cardiac Surgery perfusionists, Natalie Plokita, Ben Lamar, and Alex Vasic for their assistance with cardiopulmonary bypass in the animal surgery. Last, the authors thank the University of Chicago Human Tissue Resource Center (RRID:SCR_019199).

References

1. Wu W, He J, Shao X. Incidence and mortality trend of congenital heart disease at the global, regional, and national level, 1990-2017. *Medicine (Baltimore)*. 2020; 99:e20593.
2. Poynter JA, Eghtesady P, McCrindle BW, Walters HL, Kirshbom PM, Blackstone EH, et al. Association of pulmonary conduit type and size with durability in infants and young children. *Ann Thorac Surg*. 2013;96:1695-702.
3. Downing TE, Allen KY, Goldberg DJ, Rogers LS, Ravishankar C, Rychik J, et al. Surgical and catheter-based reinterventions are common in long-term survivors of the Fontan operation. *Circ Cardiovasc Interv*. 2017;10:e004924.
4. Rocco KA, Maxfield MW, Best CA, Dean EW, Breuer CK. In vivo applications of electrospun tissue-engineered vascular grafts: a review. *Tissue Eng Part B Rev*. 2014;20:628-40.
5. Yeung E, Inoue T, Matsushita H, Opfermann J, Mass P, Aslan S, et al. In vivo implantation of 3-dimensional printed customized branched tissue engineered vascular graft in a porcine model. *J Thorac Cardiovasc Surg*. 2020;159:1971-81.e1.
6. Fukunishi T, Best CA, Sugiura T, Opfermann J, Ong CS, Shinoka T, et al. Preclinical study of patient-specific cell-free nanofiber tissue-engineered vascular grafts using 3-dimensional printing in a sheep model. *J Thorac Cardiovasc Surg*. 2017; 153:924-32.
7. Fujita S, Yamagishi M, Kanda K, Maeda Y, Inoue T, Yamanami M, et al. Histology and mechanics of in vivo tissue-engineered vascular graft for children. *Ann Thorac Surg*. 2020;110:1050-4.
8. Loke YH, Kim B, Mass P, Opfermann JD, Hibino N, Krieger A, et al. Role of surgeon intuition and computer-aided design in Fontan optimization: a computational fluid dynamics simulation study. *J Thorac Cardiovasc Surg*. 2020;160:203-12.e2.
9. Liu X, Aslan S, Kim B, Warburton L, Jackson D, Muhuri A, et al. Computational Fontan analysis: preserving accuracy while expediting workflow. *World J Pediatr Congenit Heart Surg*. 2022;13:293-301.
10. Aslan S, Loke YH, Mass P, Nelson K, Yeung E, Johnson J, et al. Design and simulation of patient-specific tissue-engineered bifurcated right ventricle-pulmonary artery grafts using computational fluid dynamics. *2019 IEEE 19th International Conference on Bioinformatics and Bioengineering (BIBE)*; 2019. 1012-8. https://doi.org/10.1109/BIBE.2019.00188
11. Hathcock JJ. Flow effects on coagulation and thrombosis. *Arterioscler Thromb Vasc Biol*. 2006;26:1729-37.
12. Schäfer M, Kheyfets VO, Schroeder JD, Dunning J, Shandas R, Buckner JK, et al. Main pulmonary arterial wall shear stress correlates with invasive hemodynamics and stiffness in pulmonary hypertension. *Pulm Circ*. 2016;6:37-45.
13. Friesen RM, Schäfer M, Ivy DD, Abman SH, Stenmark K, Browne LP, et al. Proximal pulmonary vascular stiffness as a prognostic factor in children with pulmonary arterial hypertension. *Eur Heart J Cardiovasc Imaging*. 2019;20:209-17.
14. Soulat G, Scott MB, Pathrose A, Jarvis K, Berhane H, Allen B, et al. 4D flow MRI derived aortic hemodynamics multi-year follow-up in repaired coarctation with bicuspid aortic valve. *Diagn Interv Imaging*. 2022;103:418-26. https://doi.org/10.1016/j.diii.2022.04.003
15. Biglino G, Cosentino D, Steeden JA, De Nova L, Castelli M, Ntsinjana H, et al. Using 4D cardiovascular magnetic resonance imaging to validate computational fluid dynamics: a case study. *Front Pediatr*. 2015;3:107.
16. Eshtehardi P, Brown AJ, Bhargava A, Costopoulos C, Hung OY, Corban MT, et al. High wall shear stress and high-risk plaque: an emerging concept. *Int J Cardiovasc Imaging*. 2017;33:1089-99.
17. Millon A, Sigovan M, Boussel L, Mathevet JL, Louzier V, Paquet C, et al. Low WSS induces intimal thickening, while large WSS variation and inflammation induce medial thinning, in an animal model of atherosclerosis. *PLoS One*. 2015;10:e0141880.
18. Barker AJ, van Ooij P, Bandi K, Garcia J, Albaghdadi M, McCarthy P, et al. Viscous energy loss in the presence of abnormal aortic flow: energy loss in the presence of abnormal aortic flow. *Magn Reson Med*. 2014;72:620-8.
19. Otsu N. A threshold selection method from gray-level histograms. *IEEE Trans Syst Man Cybern*. 1979;9:62-6.
20. Liu X, Aslan S, Hess R, Mass P, Olivieri L, Loke YH, et al. Automatic shape optimization of patient-specific tissue engineered vascular grafts for aortic coarctation. *Annu Int Conf IEEE Eng Med Biol Soc*. 2020; 2020:2319-23.
21. Aslan S, Mass P, Loke YH, Warburton L, Liu X, Hibino N, et al. Non-invasive prediction of peak systolic pressure drop across coarctation of aorta using computational fluid dynamics. *Annu Int Conf IEEE Eng Med Biol Soc*. 2020;2020: 2295-8.
22. Liu X, Kim B, Loke YH, Mass P, Olivieri L, Hibino N, et al. Semi-automatic planning and three-dimensional electrospinning of patient-specific grafts for Fontan surgery. *IEEE Trans Biomed Eng*. 2022;69:186-98.
23. Matsushita H, Inoue T, Abdollahi S, Yeung E, Ong CS, Lui C, et al. Corrugated nanofiber tissue-engineered vascular graft to prevent kinking for arteriovenous shunts in an ovine model. *JVS Vasc Sci*. 2020;1:100-8.
24. Luo J, Lei H, Shen L, Yang R, Pu Q, Zhu K, et al. Estimation of growth curves and suitable slaughter weight of the Liangshan pig. *Asian-Australas J Anim Sci*. 2015; 28:1252-8.
25. Keifenheim JJ. *A Study of the Hydrostatic and Hydrodynamic Properties of Aeoliscus straigatus. Dissertation*. University of Wisconsin-Milwaukee; 2016.
26. Feng Y, Wu J, Zhu H, Wang Q, Li T, Xu Y, et al. Three-dimensional measurement and analysis of benign prostatic hyperplasia. *Transl Androl Urol*. 2021;10: 2384-96.
27. Mandell JG, Loke YH, Mass PN, Cleveland V, Delaney M, Opfermann J, et al. Altered hemodynamics by 4D flow cardiovascular magnetic resonance predict exercise intolerance in repaired coarctation of the aorta: an in vitro study. *J Cardiovasc Magn Reson*. 2021;23:99.
28. Schulz-Menger J, Bluemke DA, Bremerich J, Flamm SD, Fogel MA, Friedrich MG, et al. Standardized image interpretation and post-processing in cardiovascular magnetic resonance–2020 update: Society for Cardiovascular Magnetic Resonance (SCMR): board of trustees task force on standardized post-processing. *J Cardiovasc Magn Reson*. 2020;22:19.
29. Hope MD, Hope TA, Meadows AK, Ordovas KG, Urbania TH, Alley MT, et al. Bicuspid aortic valve: four-dimensional MR evaluation of ascending aortic systolic flow patterns. *Radiology*. 2010;255:53-61.
30. Schnell S, Smith DA, Barker AJ, Entezari P, Honarmand AR, Carr ML, et al. Altered aortic shape in bicuspid aortic valve relatives influences blood flow patterns. *Eur Heart J Cardiovasc Imaging*. 2016;17:1239-47.
31. Trusty PM, Wei ZA, Slesnick TC, Kanter KR, Spray TL, Fogel MA, et al. The first cohort of prospective Fontan surgical planning patients with follow-up data: how accurate is surgical planning? *J Thorac Cardiovasc Surg*. 2019;157: 1146-55.
32. Chang HW, Kim SH, Hakim AR, Chung S, Kim DJ, Lee JH, et al. Diameter and growth rate of the thoracic aorta—analysis based on serial computed tomography scans. *J Thorac Dis*. 2020;12:4002-13.
33. Dolan JM, Kolega J, Meng H. High wall shear stress and spatial gradients in vascular pathology: a review. *Ann Biomed Eng*. 2013;41:1411-27.
34. Brun H, Bugge RAB, Suther LKR, Birkeland S, Kumar R, Pelanis E, et al. Mixed reality holograms for heart surgery planning: first user experience in congenital heart disease. *Eur Heart J Cardiovasc Imaging*. 2019;20:883-8.
35. Munawar A, Li Z, Kunjam P, Nagururu N, Ding AS, Kazanzides P, et al. Virtual reality for synergistic surgical training and data generation. *Comput Methods Biomech Biomed Eng Imaging Vis*. 2021;10:366-74.

Key Words: tissue-engineered vascular grafts, displacement, wall shear stress, computational fluid dynamics, center of gravity, hemodynamics, surgical planning

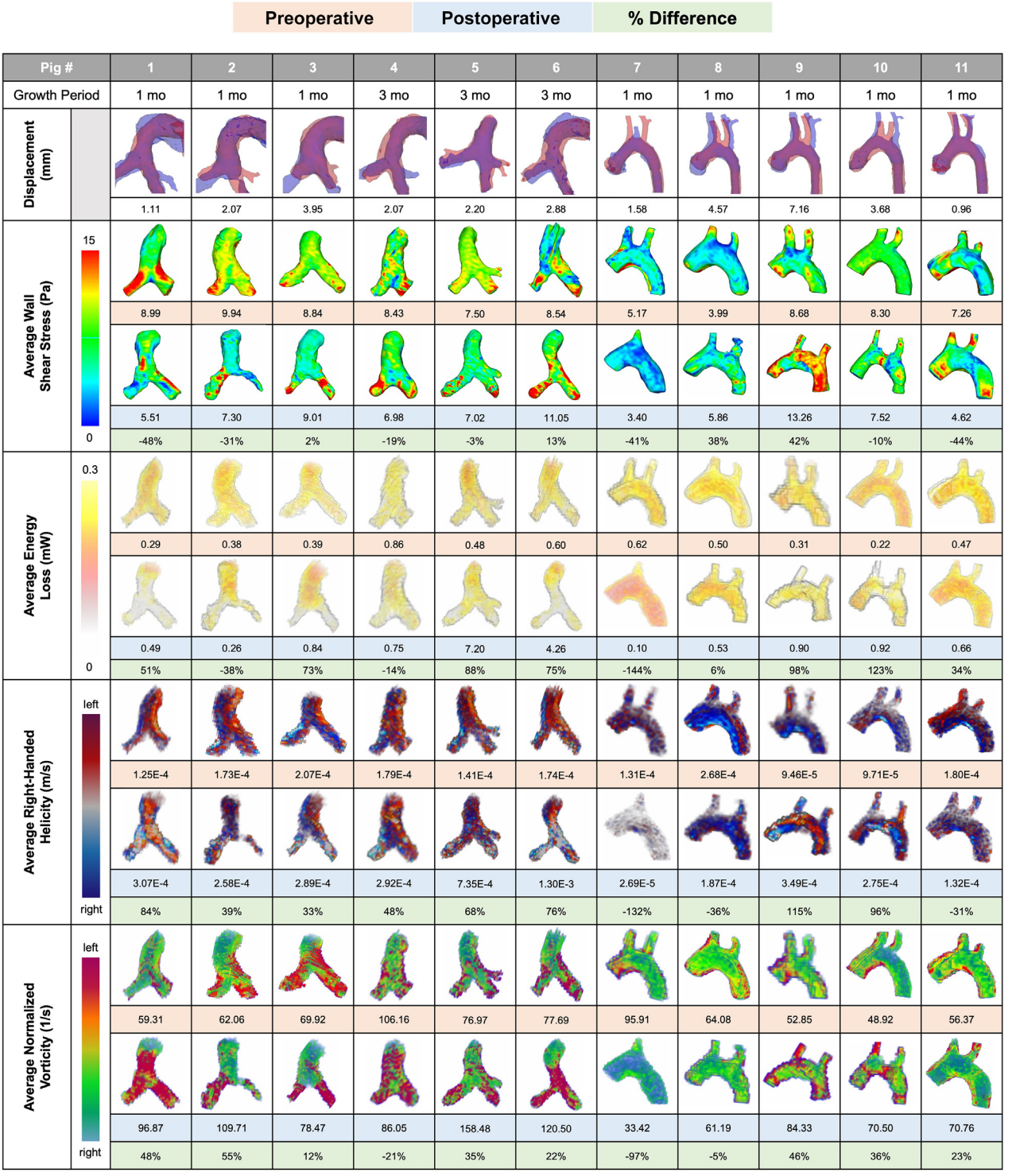

FIGURE E1. Displacement, wall shear stress, energy loss, helicity, and vorticity for all 11 porcine models. Hemodynamic images reflect pre- (*top*) and postoperative (*bottom*) vasculature at systole. Note that images are 2-dimensional, which might not fully display the 3D data.